Quasi-brittle Fracture Mechanics of Human Cortical Bone: Implications to Bone Health

Glynn Gallaway[a], Rachel K. Surowiec[b,c], Matthew R. Allen[d,e], Joseph M. Wallace[b], Laura J. Pyrak-Nolte[f], John Howarter[g], Thomas Siegmund[a,*]

[a]*School of Mechanical Engineering, Purdue University,*
[b]*Department of Biomedical Engineering, Indiana University Purdue University Indianapolis,*
[c]*Department of Radiology and Imaging Sciences, Indiana University School of Medicine,*
[d]*Department of Anatomy, Cell Biology, and Physiology, Indiana University School of Medicine,*
[e]*Roudebush Veterans Administration Medical Center,*
[f]*Department of Physics and Astronomy, Purdue University,*
[g]*School of Materials Engineering, Purdue University,*

Abstract

Human bone fracture behavior and toughness are of interest to both the engineering and clinical orthopedic communities as new treatments for bone diseases, such as osteoporosis, are developed. Much of the work on bone fracture has used linear elastic fracture mechanics (LEFM) or the J-integral. These works indicate that bone has a large resistance to fracture that declines with age. However, there is large variability among current studies in results, specimen size, donor tissue demographics, and experimental methods. Here, a quasi-brittle fracture mechanics framework is introduced to evaluate cortical bone fracture, supported by in-situ loading and 3D imaging. Quasi-brittle fracture mechanics can provide insights into the behavior of cortical bone beyond LEFM approaches as we introduce measurements across multiple length scales into the fracture characterization of bone. Quasi-brittle fracture mechanics allows tools for further development of treatments to address both bone quantity and bone quality.

Keywords: Bone, Fracture, Bone Quality, Bone Quantity

*Corresponding Author at: 585 Purdue Mall, West Lafayette, IN 47906, USA
Email address: siegmund@purdue.edu (Thomas Siegmund)

1. Introduction

Recent census reports indicate that the US population is older than ever before, thereby increasing the population at risk for bone fractures [1]. Fragility fractures in those of advanced age are linked to decreased quality of life and increased mortality risk [2]. However, treatments for osteoporosis are among the least effective when compared to other common diseases [3]. The development of effective methods to decrease fracture risk is critical to advancing health outcomes in the current population and reducing burden on healthcare infrastructure. Assessing the need for clinical intervention in bone diseases such as osteoporosis has often relied on measurements of bone mineral density (BMD) and its implied strength through Dual-energy X-ray absorptiometry (DEXA). However, DEXA imaging has been previously reported to be imperfect in assessing fracture risk [4, 5]. Fracture mechanics can provide an alternative approach to understanding other factors leading to fragility fracture beyond density and strength [6].

Linear elastic fracture mechanics (LEFM) has typically been used to report fracture behavior in bone, either through stress intensity factors, critical distance theory, or via the J-integral. Stress intensity factors are a common tool for characterizing toughness and have been used in several studies with a variety of tissues and experimental methods with a large range in results [7]. The theory of critical distances, derived from LEFM, has been previously applied in fracture mechanics of bone and suggests that the microstructure influences toughness [8]. However, LEFM assumes that no significant damage occurs before peak load and the material is linear elastic which is untrue of bone. The J-integral has been commonly used in fracture experiments of bone to demonstrate its strong resistance to fracture through the steep rise in J as a crack grows relative to other materials and bone's individual material components [9]. The J-integral does account for plasticity and other non-linear fracture behavior, but does not include a length scale and cannot characterize fracture behavior near the tip. J-integral calculations following ASTM E1820 [10] may also over-predict bone toughness [11].

Fracture toughness of bone has been found to differ with respect to age [12, 13, 14, 15], disease [16], and anatomical direction [7]. Regardless, bone exhibits exceptional toughness and resistance to fracture due to the extrinsic and intrinsic toughening mechanisms present across hierarchical length scales [17]. Of particular interest to this study, are toughening mechanisms derived from the structure and interfaces in bone, such as microcracking, crack deflec-

tion at the cement line, crack bridging, and osteon pullout [18, 19, 20]. The accumulation of damage develops a fracture process zone (FPZ) in cortical bone. While much research has employed LEFM to describe bone toughness, the relative size of the FPZ is significant compared to both micro-structural and whole bone length scales and informs the need for an alternative approach.

Quasi-brittle fracture mechanics (QBFM) has been developed to analyze fracture in materials that possess a relatively large FPZ and exhibit a size effect [21, 22]. QBFM has been implemented in several materials, such as concrete [21, 23], fiber composites [24], ceramics [25, 22], and rock [26, 27]. QBFM has also been used to characterize bovine bone [28]. Some measurements in the human humerus point to an FPZ size in the longitudinal direction of 5-7 mm [29], but no measurements have been reported for human cortical bone in the transverse direction. To determine size effects on strength and/or toughness in engineering materials, multi-specimen approaches are typically used by 1) Evaluating geometrically similar samples of multiple sizes [28, 23], or 2) evaluating samples of the same size with multiple crack lengths [23]. Such approaches become challenging to execute in bone due to the limited material availability of human bone tissue for experiments, high subject specificity, and biological limitations on tissue size. This study aims to apply QBFM to human cortical bone using an alternative approach made possible by in-situ loading with 3D imaging. QBFM further allows interpretation of bone quality and bone quantity contributions to fracture toughness.

2. Materials and Methods

2.1. Materials

The diaphysis of a human (92-year-old, male) cadaveric femur was obtained through the Indiana University School of Medicine Anatomical Donation Program. A 3D scan of the femur revealed the largest cortical thickness at the distal mid-diaphysis. A section of the femur was extracted at this location. In this section, the average cortical thickness in the section was $\hat{t}_c = 6.9$ mm. Considering cortical wall curvature and internal porosities, the largest prismatic bars that could be extracted from the section were of nominal size 4.0 mm $\times$ 4.0 mm $\times$ 28.0 mm. Specimen were cut using a low-speed saw equipped with a cBN blade (Buehler, Illinois, USA) and ground to square. The sample of interest was dissected from the lateral posterior cortex and

was of actual dimensions: $B = 4.1$ mm, $D = 3.9$ mm, $L = 28.0$ mm. An edge notch, of depth $a_0 = 1.7$ mm, was introduced into the endosteal face of the SEN(B) specimen using a low-speed saw equipped with a 200 μm thick diamond blade (Buehler, Illinois, USA). The bone volume to total volume ratio (BV/TV) of the un-notched beam was determined using a SkyScan 1176 μ-Computed Tomography system (Brucker, Massachusetts, USA; 16.9 μm resolution) and segmented with Simpleware ScanIP (Synopsys, California, USA). BV/TV in the specimen half above the notch was 88%.

The elastic modulus of bone matrix was taken to be $E_0 = 19.08$ GPa in the longitudinal direction [30]. Osteon diameter, On.Dm, was measured from a polished slice of the beam post-fracture (Fig. 5A) by backscatter SEM as the average minimum Feret diameter of the outlined osteons (Fig. 5B) and found to be On.Dm = 195.0 μm [31].

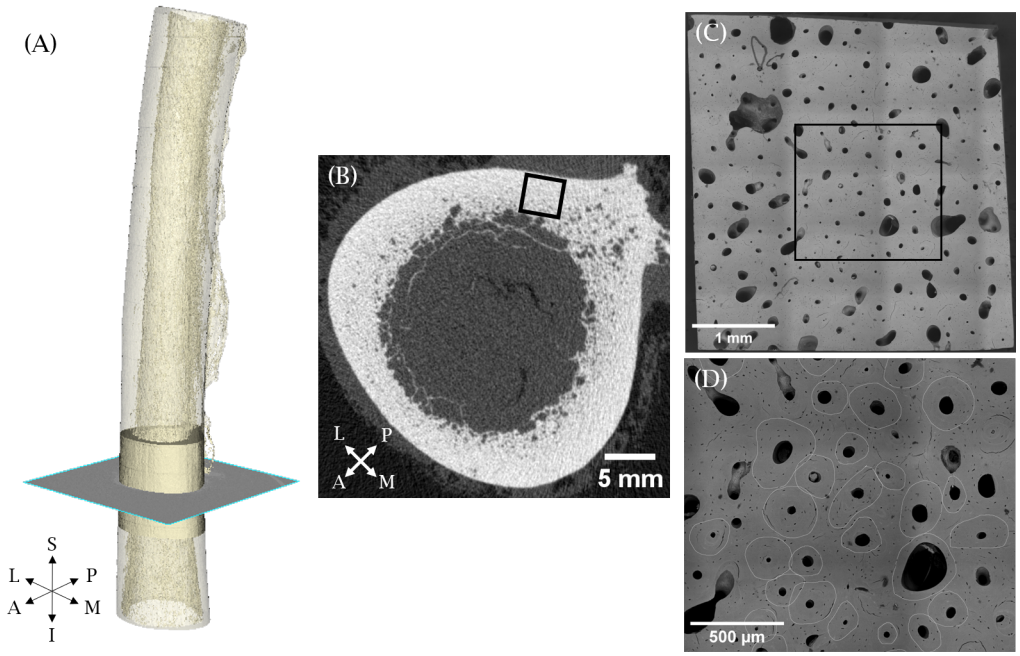

Figure 1: (A) 3D reconstruction of the femoral shaft (transparent) with section where beam was extracted (opaque). (B) Cross-section shown in (A) of femoral shaft with approximate beam location outlined. (C) Backscatter SEM of beam cross-section. (D) Portion of backscatter SEM indicated in (C) showing outline of osteons used to measure On.Dm (white).

The sample presented is a control from a larger study on the pharmaceu-

tical treatment of bone. Consequently, the specimen was incubated for 14 days at 37 °C in a solution of phosphate buffered saline supplemented with 1% penicillin-streptomycin and 0.04% vol/vol dimethyl sulfoxide, [32]. After, the sample was kept frozen at -20 °C, and defrosted at 4 °C overnight before fracture experiments.

2.2. Fracture Experiment with 3D Imaging

In-situ fracture experiments were conducted in 3-point bending with a Deben CT5000N load cell (Deben, Bury St. Edmunds, UK) in a Zeiss XRADIA 510 Versa 3D X-Ray microscope (Carl Zeiss AG, Baden-Württemberg, Germany). The 3-point bending frame had a span $S = 20$ mm with rigid X-Ray transparent glassy carbon supports (diameter 5.0 mm) to avoid image artifacts. To maintain hydration, the beam was wrapped in plastic film with a slit around the notch. Displacement was applied at a rate of 0.1 mm/min up to the approximate onset of non-linearity. At that instant, the displacement was held constant and the first 3D image was obtained. Subsequently, the displacement was increased at the same rate until a load increase of 10 N was observed and another image was obtained. This sequence was repeated until peak load and resulted in six 3D images. 3D X-ray images were acquired with a resolution of 4.5 μm using an exposure time of 5 s for the 801 projections at 120 kV, 10W, 4× objective, and a LE2 filter. For the full imaging sequence, the estimated radiation dosage by the manufacturer was 54 Gy, which is on the order of magnitude found not to influence the mechanical or fracture properties of bone [33].

Applied force data was obtained from the load cell of the Deben system. X-Ray projections were processed through XRADIA Scout-and-Scan Reconstructor and then analyzed using Simpleware ScanIP. A recursive Gaussian smoothing filter ($\sigma = 1$ pixel) was applied to reduce image artifacts. Crack mouth opening displacement, $CMOD$, was obtained from 3D image measurement tools in ScanIP. FPZ length, l_{FPZ}, was determined, with respect to pixel size, as the distance from the first image slice orthogonal to the initial crack plane containing a partially separated crack to the last image slice containing a visible crack. The length of the fully separated crack growth, Δa_{full}, can be similarly measured from the notch root to the last slice of a fully separated crack; then a total effective crack growth can be determined:

$$\Delta a_{eff} = \Delta a_{full} + l_{FPZ} \tag{1}$$

2.3. Linear Elastic Fracture Mechanics - LEFM

Evaluation of the tissue toughness can begin from ASTM guidelines for fracture experiments [10]. The linear elastic fracture toughness, G_{LEFM} is:

$$G_{LEFM}(D) = \frac{P_{max}^2}{E'\rho D^3} g_{(S/W)}(\alpha_0) \tag{2}$$

Here, P_{max} is the maximum measured load in the experiment, and $B^2 D = \rho D^3$. The plane strain elastic modulus is $E' = E_0(BV/TV)/(1-\nu^2)$. The normalized initial notch depth is $\alpha_0 = a_0/D$, where a_0 is the initial notch depth. The configuration function g depends on specimen and support geometry. Configuration functions are most commonly provided for stress intensity factors, $K = \sqrt{(G/E')}$. Then, the configuration factor for calculations of energy release rates is $g = k^2$. A comprehensive solution of $k_{(S/W)}(\alpha)$ for the SEN(B) specimen in a 3-point bend configuration is given in [34]. For the span-to-width ratio ($S/W = 5$) the following expression is provided:

$$k_5(\alpha) = \frac{\sqrt{\alpha}}{(1-\alpha)^{3/2}(1+3\alpha)}[2.062 + 1.166\alpha - 0.966\alpha^2 + 0.388\alpha^3] \tag{3}$$

2.4. Quasi-Brittle Fracture Mechanics - QBFM

In materials that are not perfectly brittle, an FPZ of finite length, l_{FPZ}, is present at the crack tip. Within that zone, the material transitions from being fully intact to fully separated. The maximum extent of l_{FPZ} is reached at the instance of P_{max} and the elastic equivalent crack extension can be estimated as $c = \max(l_{FPZ})/2$, [35]. A factor of 1/2 is used to account for a linear decay of traction from the crack tip to the fully separated crack. A normalized effective crack length at P_{max} is defined as:

$$\alpha_{eff} = \frac{1}{D}\left(a_0 + c\right) \tag{4}$$

Then, a corrected toughness measure for the quasi-brittle fracture mechanics approach, G_{QBFM}, can be established by accounting for the fracture process zone.

$$G_{QBFM} = \frac{P_{max}^2}{E'\rho D^3} g(\alpha_{eff}) \tag{5}$$

The two toughness measures can be connected if a linear extrapolation approach is used [35]. Then, the configuration function with respect to the effective crack length in the large limit can be defined as

$$g(\alpha_{eff}) = g(\alpha_0) + g'(\alpha_0)\frac{c_f}{D} \tag{6}$$

where g' is $(dg/d\alpha)$. Combining Eq. 6 with Eqs. 2 and 5 leads to an approximation for the quasi-brittle fracture toughness G^{lin}_{QBFM}:

$$G^{lin}_{QBFM} = G_{LEFM}\left[1 + \frac{c}{D}\frac{g'(\alpha_0)}{g(\alpha_0)}\right] = G_{LEFM}\left(1 + \frac{1}{\beta}\right) \tag{7}$$

In Eq. 7 the term $\beta = \frac{D}{c}\frac{g(\alpha_0)}{g'(\alpha_0)}$ plays a central role and characterizes the degree to which a specimen is considered to be either brittle (such that LEFM applies, $\beta > 10$), quasi-brittle (such that QBFM applied, $0.1 < \beta < 10$) or not crack sensitive (such that neither LEFM or QBFM apply, $\beta < 0.1$) [36]. The existence of a finite length FPZ causes G_{LEFM} and G_{QBFM} to be dependent on specimen size. Typically, for engineering materials, a size-independent fracture toughness, G_f, is determined by extrapolation to infinite specimen size ($d \to \infty$) using Eq. 7, [35]. The value of G_f is then considered a material property. However, for human cortical bone, such an extrapolation is not viable. Due to the biological constraints on the cortical thickness, it is not possible to increase the specimen dimensions much beyond D as would be needed for the determination of G_f.

3. Results

Figure 2 depicts the Force - $CMOD$ record from the experiment, and shows a response typical for quasi-brittle solids. After an initial settling period, the response of the specimen is linear, followed by a nonlinear response initiating around P_3 with a load maximum, and subsequent load reduction to failure.

Figure 3 depicts the reconstruction of the 3D X-ray image at load stage $P_6 = 62.3$ N. Movies depicting the reconstructed Haversian Canal and crack structure are provided as Supplementary Material. Reconstructed images provided here are larger than others have reported using smaller samples with cross-sections on the scale of 2 mm or less [37, 7, 38, 14] The crack becomes fully separated from the induced notch at peak load (P_5), at which point the fracture process zone is fully developed and of constant length. Observed in 3D, the crack is shown to be tortuous and interacts with the microstructure at the length scale of On.Dm. Crack bridging (Fig. 3D), crack deflection (Fig. 3B-C), and osteon pullout (Fig. 3A) are observed. The crack extends further internally than at the surface due to plane strain conditions as compared to plane stress conditions at the beam face (see Fig.

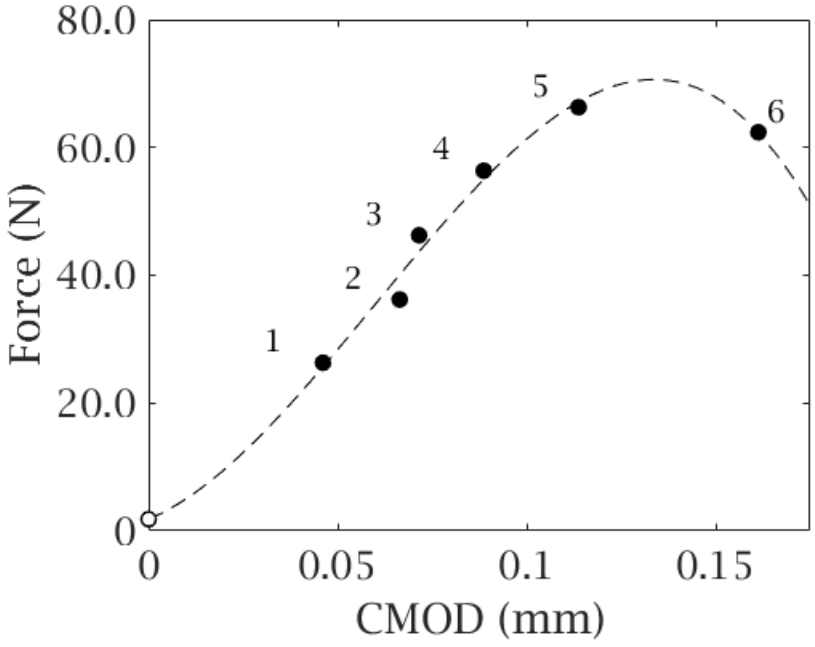

Figure 2: Force, P, vs. Crack Mouth Opening Displacement, $CMOD$, for 3-point bending of the SEN(B) specimen. Data points (dots) for each load image pair (#), $P_{max} = P_5 =$ 66.3 N. Fit to data (dashed line).

4). The crack extends in the transverse direction and deflects longitudinally in areas where cement lines are expected based on Haversian canals and osteon diameter. Based on the sequence of reconstructed 3D images at each load step, development of the FPZ can be tracked (Fig. 4). FPZ growth begins around the onset of linearity (P_3, see Fig. 2) and plateaus in size at peak load (P_5). The FPZ begins internally and extends to the surface after increased load. In the sample, $\max(l_{FPZ}) = 348$ μm. As the osteon emerges as the microstructural feature determining crack growth, we express $\max(l_{FPZ}) = \eta \cdot \text{On.Dm}$, with $\eta = 1.8$ for the present specimen. Using Eq. 2 with the maximum measured force (Fig. 2, $P_{max} = P_5$) and $\alpha_0 = 0.41$, the LEFM energy release rate value is $G_{LEFM} = 0.46$ N/mm. At peak load, from Fig. 4, one determines $c = 174$ μm which results in $\alpha_{eff} = 0.46$. Then, the quasi-brittle fracture toughness accounting for the presence of the FPZ (Eq. 5) is $G_{QBFM} = 0.60$ N/mm. The linearization of Eq. 5 to Eq. 7 provides $G^{lin}_{QBFM} = 0.58$ N/mm. Furthermore, $\beta = 3.9$, is well in the range of quasi-

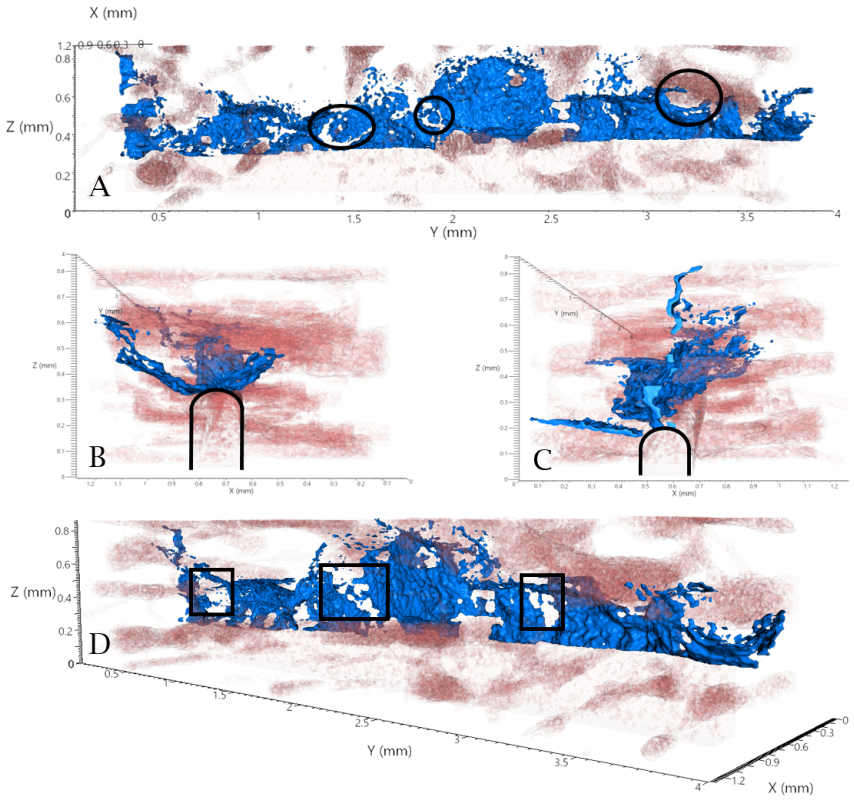

Figure 3: Reconstructed 3D image of the cortical bone specimen under mechanical loading at $P_6 = 62.3$ N. Haversian canals (red) and the material separation induced by mechanical loading (blue). (a) A view orthogonal to the plane of the initial notch with examples of osteon pullout (circled). (B,C) Views parallel to the front of the initial notch (outlined) from each side, (D) Perspective view with examples of crack bridging (boxed).

brittle fracture conditions. Hypothetically, a specimen size of $d > 30$ mm would be needed to obtain LEFM conditions, a condition that cannot be fulfilled as $t_c = 6.9$ mm.

4. Discussion

Cortical bone extracted from the femur of a 92-year-old male emerges as a quasi-brittle solid with G_{LEFM} markedly different from G_{QBFM}. This is confirmed by pronounced FPZ at the crack tip which introduces a size dependence of the fracture characteristics. Prior fracture mechanics studies on transverse fracture toughness of cortical bone have considered smaller

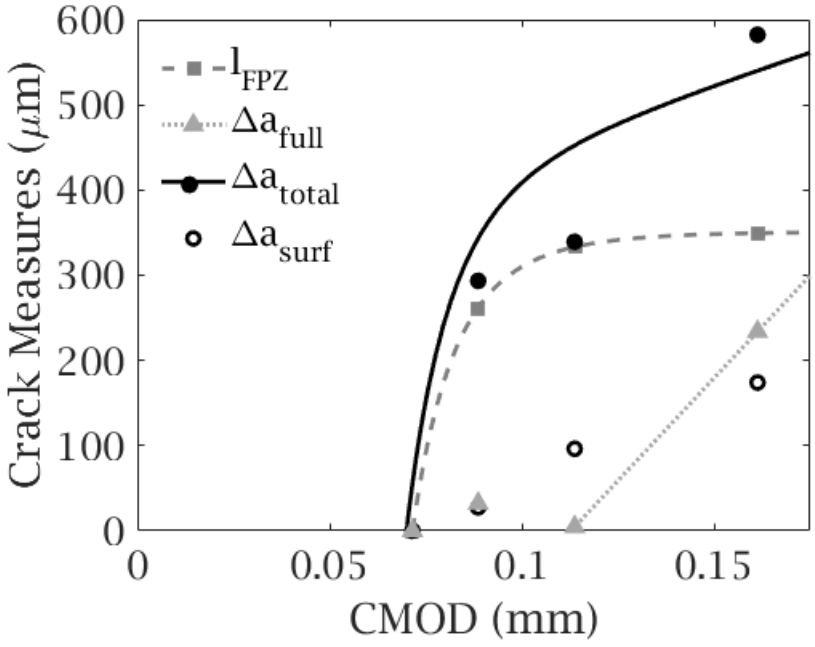

Figure 4: Crack measurements with respect to loading state (#). The fracture process zone grows up to peak load and plateaus at $l_{FPZ} = 348\mu$m. As the FPZ stops growing, the fully separated crack begins to grow. Together these contribute to the total crack growth. The crack visible at the beam surface, Δa_{surf}, is considerably smaller as compared to that seen internally.

specimen dimensions and therefore detected a rather ductile behavior [7]. Such a behavior is the result of the dominant non-linearity of the FPZ. The QBFM approach as applied here indicates that even for the practically largest specimen size possible in the human femur, there is a significant size effect on fracture toughness. Investigation of the fracture surfaces, in conjunction with 3D reconstructions, can lead to insight into the mechanical and biological interactions. Figure 5 shows part of the fracture surface created in the experiment; Distinct height differences emerge at cement lines in the direction of crack propagation. Osteons emerge as the fundamental building blocks of the bone tissue, and the failure of the cement line and subsequent osteon fracture determines the FPZ. Discussions on treatment of bone disease often focus on addressing bone quantity or bone quality. Both of these areas encompass a large field of contributing and overlapping variables. The QBFM framework allows these areas to be addressed in terms of the individ-

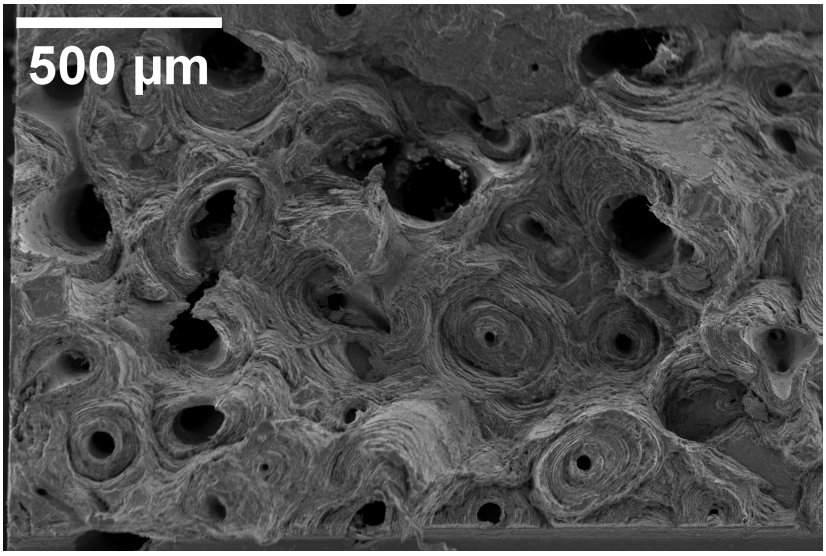

Figure 5: Post-mortem SEM of fracture surface. The crack propagates upward from the machined notch and height differences appear as a result of crack deflection at cement lines and osteon pullout.

ual variables' contribution to fracture toughness. To assess the mechanical resilience of the mid-section of the femur bone, Eq. 7 is rewritten:

$$G_{bone} = \frac{G_{QBFM}^{lin}}{\left[1 + \frac{\eta \cdot \text{On.Dm}}{\hat{t}_c} \frac{\tilde{g}'(\tilde{\alpha}_0)}{\tilde{g}(\tilde{\alpha}_0)}\right]} \tag{8}$$

Thereby, the initial crack length is that of a naturally occurring defect,

$$\tilde{a}_0 \propto \text{On.Dm} \tag{9}$$

$$\tilde{\alpha}_0 = \tilde{a}_0 / t_c \tag{10}$$

The functions $\tilde{g}(\tilde{\alpha}_0)$ and $\tilde{g}'(\tilde{\alpha}_0)$ are the configuration function and its derivative, respectively, for such defects in the long bone, which can be approximated by known configuration functions (e.g. a surface crack in a thick-walled pipe under bending [39, 40]). The factor η represents the length of the FPZ relative to On.Dm. The apparent toughness of the femur, G_{bone}, can be used together with the LEFM approach, Eq. 2, to determine the maximum load allowable, P_{allow}, in such bone

$$P_{allow} = \sqrt{\frac{G_{bone} E' \tilde{\rho} t_c^3}{\tilde{g}(\tilde{\alpha}_0)}} \tag{11}$$

where $\tilde{\rho}$ is a geometry factor for the femur cross-section. We propose to use Eqs. 8 and 11 as a framework for understanding the combined effects of bone quantity and bone quality on bone resilience. The obvious objective is to increase P_{allow} by increasing G_{bone} such that toughness is increased and fracture risk decreases. The equation for G_{bone} is coupled both mathematically (e.g. $\tilde{g}(\tilde{\alpha_0})$ is dependent on t_c) and biologically (e.g. remodeling balances both t_c and On.Dm), but the individual factors can be evaluated for their effect.

Aging often reduces bone quantity; reduction of cortical thickness [41] and BV/TV [42] are observed. Reducing t_c will result in a reduced P_{allow} directly through the t_c^3 term, by reducing G_{bone} due to the $1/t_c$ term, and by increasing $\tilde{\alpha}_0$ and thus also increasing both g and g'/g. A loss in BV/TV due to increased Haversian canal diameter reduces the resilience of the individual osteon to failure and reduces G_{QBFM} and P_{allow}.

Measures of bone quality also change with age; On.Dm decreases [31], the size and number of in-vivo microcracks increases [43], and non-enzymatic collagen cross-linking and mineralization also increase [44, 45]. Decreases in On.Dm would reduce the FPZ length and thus reduce G_{bone} and P_{allow}. As micro-crack size and number increases, at least in part due to sluggish remodeling, in a similar manner to the effects of BV/TV, $\tilde{\alpha}_0$ increases and G_{QBFM} and P_{allow} are reduced. Increased non-enzymatic cross-linking in collagen reduces the deformation capacity of the individual osteon and the bone matrix as a whole. Such cross-linking reduces bones ability to form crack bridges and extend l_{FPZ} by η, leading to a reduction in G_{bone} and P_{allow}. Increased mineralization moves bone towards a more brittle composition which would alter β and lead to decreased G_{bone} and P_{allow}.

Anti-resorptive drugs, such as bisphosphonates and Denosumab are common tools for treating bone loss, and their effects on several of the contributing variables in equation 8 have been studied. Cortical thickness in the femoral shaft is reported to not be influenced by bisphosphonate treatment [46, 47] or exercise [48]. However, some research indicates apparent cortical thickness increased due to Alendronate and Denosumab treatment [49]. Denosumab has shown some effectiveness in changing cortical thickness at the trochanter [50]. Denosumab is also linked to increased BV/TV at the proximal femoral shaft in women with osteoporosis [51]. In terms of bone quality, bisphosphonate treatment has been shown to not affect the degree of crack deflection [52]. Bisphosphonate treatment has been used to reduce cortical porosity, however, this is often achieved by blocking bone resorption

and remodeling which can allow damage to accumulate and drive up the initial defect size [53]. In the treatment of osteoporosis, bisphosphonates have been linked to increased osteon diameter as compared to same-aged peers, yet a cause is unclear [54]. Bisphosphonates can induce hypermineralization which further increases brittleness [44]. Overall, anti-resorptive pharmaceutical treatments may reduce fracture risk by increasing t_c and On.Dm, but this effect may be counteracted by increases in microdamage and mineralization.

Parametric studies have shown that cement line, interstitial bone tissue, and osteon bone tissue properties have a significant impact on the crack path and degree of osteon deflection [55, 56]. Additionally, the osteon density and material heterogeneity impact fracture properties in experimental and computational studies [57, 58]. The bone ultrastructure, a function of the mineral, collagen, and water content, has been found to affect toughness [59]. Improved toughness and post-yield behavior have been observed in canine and murine bone treated by raloxifene or calcitonin which alters bone water content through non-cell mediated mechanisms [32, 60]. While On.Dm is somewhat dictated by biological sex and age, weight and local strains induced by physical activity can be controlled to change On.Dm [31, 61].

The presented work is limited to a single specimen but motivates the need to incorporate size effect into the evaluation of fracture toughness of human bone. The results show a lower toughness than those typically reported, but are derived from a sample of advanced age, of larger specimen dimensions than typical, and detect crack initiation earlier - all factors which could contribute to the lower measured toughness. This sample is exposed to air and drying effects during testing which does not represent anatomic conditions and could alter the true tissue toughness [62].

5. Conclusions

Addressing bone health is key to improving the quality of life among those of advanced age and reducing the burden on healthcare infrastructure. This study shows that a fracture process zone of significant size exists in transverse fracture of the femur. Using quasi-brittle fracture mechanics, a size-accurate toughness can be obtained by accounting for the fracture process zone size in addition to the linear elastic fracture mechanics analysis. The QBFM framework allows for discussion on the relevant structural variables affecting bone quantity and quality.

6. Conflict of interest statement

The authors declare no conflicts.

7. Acknowledgements

This work is supported by NSF (CMMI) grant 1952993. G.G. is supported by NSF-GRF DGE-1842166 and Purdue Doctoral Fellowship. We acknowledge the 3D X-Ray Microscope Facility in the Department of Physics, Purdue University, supported by the EVPRP 2017 Major Multi-User Equipment Program.

References

[1] U. C. Bureau, U.s. older population grew from 2010 to 2020 at fastest rate since 1880 to 1890, 2023.

[2] G. G. Teng, J. R. Curtis, K. G. Saag, Mortality and osteoporotic fractures: is the link causal, and is it modifiable?, Clinical and experimental rheumatology 26 (2008) S125–S137.

[3] S. Leucht, B. Helfer, G. Gartlehner, J. M. Davis, How effective are common medications: A perspective based on meta-analyses of major drugs, BMC Medicine 13 (2015) 1–5. doi:10.1186/S12916-015-0494-1.

[4] J. A. Kanis, O. Johnell, A. Oden, B. Jonsson, C. D. Laet, A. Dawson, Risk of hip fracture according to the world health organization criteria for osteopenia and osteoporosis, Bone 27 (2000) 585–590. doi:10.1016/S8756-3282(00)00381-1.

[5] Y. Lu, H. K. Genant, J. Shepherd, S. Zhao, A. Mathur, T. P. Fuerst, S. R. Cummings, Classification of osteoporosis based on bone mineral densities, Journal of Bone and Mineral Research 16 (2001) 901–910. doi:10.1359/JBMR.2001.16.5.901.

[6] D. Dapaah, D. R. Martel, F. Iranmanesh, C. Seelemann, A. C. Laing, T. Willett, Fracture toughness: Bridging the gap between hip fracture and fracture risk assessment, Current Osteoporosis Reports 21 (2023) 253–265. doi:10.1007/S11914-023-00789-4.

[7] K. J. Koester, J. W. Ager, R. O. Ritchie, The true toughness of human cortical bone measured with realistically short cracks, Nature Materials 2008 7:8 7 (2008) 672–677. doi:10.1038/nmat2221.

[8] S. Kasiri, D. Taylor, A critical distance study of stress concentrations in bone, Journal of Biomechanics 41 (2008) 603–609. doi:10.1016/J.JBIOMECH.2007.10.003.

[9] E. A. Zimmermann, M. E. Launey, R. O. Ritchie, The significance of crack-resistance curves to the mixed-mode fracture toughness of human cortical bone, Biomaterials 31 (2010) 5297–5305. doi:10.1016/J.BIOMATERIALS.2010.03.056.

[10] ASTM, E1820 – 08a standard test method for measurement of fracture toughness, 2008.

[11] D. Dapaah, T. Willett, A critical evaluation of cortical bone fracture toughness testing methods, Journal of the Mechanical Behavior of Biomedical Materials 134 (2022) 105419. doi:10.1016/J.JMBBM.2022.105419.

[12] R. K. Nalla, J. J. Kruzic, J. H. Kinney, R. O. Ritchie, Effect of aging on the toughness of human cortical bone: evaluation by r-curves, Bone 35 (2004) 1240–1246. doi:10.1016/J.BONE.2004.07.016.

[13] R. K. Nalla, J. J. Kruzic, J. H. Kinney, M. Balooch, J. W. Ager, R. O. Ritchie, Role of microstructure in the aging-related deterioration of the toughness of human cortical bone, Materials Science and Engineering: C 26 (2006) 1251–1260. doi:10.1016/J.MSEC.2005.08.021.

[14] E. A. Zimmermann, E. Schaible, H. Bale, H. D. Barth, S. Y. Tang, P. Reichert, B. Busse, T. Alliston, J. W. Ager, R. O. Ritchie, Age-related changes in the plasticity and toughness of human cortical bone at multiple length scales, Proceedings of the National Academy of Sciences of the United States of America 108 (2011) 14416. doi:10.1073/PNAS.1107966108.

[15] P. Zioupos, J. D. Currey, Changes in the stiffness, strength, and toughness of human cortical bone with age, Bone 22 (1998) 57–66. doi:10.1016/S8756-3282(97)00228-7.

[16] P. Giannoudis, C. Tzioupis, T. Almalki, R. Buckley, Fracture healing in osteoporotic fractures: Is it really different?: A basic science perspective, Injury 38 (2007) S90–S99. doi:10.1016/J.INJURY.2007.02.014.

[17] M. E. Launey, M. J. Buehler, R. O. Ritchie, On the mechanistic origins of toughness in bone, Annual Review of Materials Research 40 (2010) 25–53. doi:10.1146/ANNUREV-MATSCI-070909-104427.

[18] F. Barthelat, The fracture mechanics of biological materials, CISM International Centre for Mechanical Sciences, Courses and Lectures 608 (2023) 255–282. doi:10.1007/978-3-031-18340-9.

[19] R. K. Nalla, J. J. Kruzic, J. H. Kinney, R. O. Ritchie, Mechanistic aspects of fracture and r-curve behavior in human cortical bone, Biomaterials 26 (2005) 217–231. doi:10.1016/J.BIOMATERIALS.2004.02.017.

[20] D. Vashishth, J. C. Behiri, W. Bonfield, Crack growth resistance in cortical bone: Concept of microcrack toughening, Journal of Biomechanics 30 (1997) 763–769. doi:10.1016/S0021-9290(97)00029-8.

[21] Z. P. Bažant, Size effect in blunt fracture: Concrete, rock, metal, Journal of Engineering Mechanics 110 (1984) 518–535. doi:10.1061/(ASCE)0733-9399(1984)110:4(518).

[22] Z. P. Bažant, M. T. Kazemi, Size effect in fracture of ceramics and its use to determine fracture energy and effective process zone length, Journal of the American Ceramic Society 73 (1990) 1841–1853. doi:10.1111/J.1151-2916.1990.TB05233.X.

[23] Z. M. Wu, H. Rong, J. J. Zheng, F. Xu, W. Dong, An experimental investigation on the fpz properties in concrete using digital image correlation technique, Engineering Fracture Mechanics 78 (2011) 2978–2990. doi:10.1016/J.ENGFRACMECH.2011.08.016.

[24] N. G. Tsouvalis, K. N. Anyfantis, Determination of the fracture process zone under mode i fracture in glass fiber composites, Journal of Composite Materials 46 (2012) 27–41. doi:10.1177/0021998311401934.

[25] K. Ando, B. A. Kim, M. Iwasa, N. Ogura, Process zone size failure criterion and probabilistic fracture assessment curves for ceramics, Fatigue Fracture of Engineering Materials Structures 15 (1992) 139–149. doi:10.1111/J.1460-2695.1992.TB00044.X.

[26] M. Moazzami, M. R. Ayatollahi, A. Akhavan-Safar, Assessment of the fracture process zone in rocks using digital image correlation technique: The role of mode-mixity, size, geometry and material, International Journal of Damage Mechanics 29 (2020) 646–666. doi:10.1177/1056789519871334/.

[27] S. P. Morgan, C. A. Johnson, H. H. Einstein, Cracking processes in barre granite: Fracture process zones and crack coalescence, International Journal of Fracture 180 (2013) 177–204. doi:10.1007/S10704-013-9810-Y.

[28] K. T. Kim, Z. P. Bažant, Q. Yu, Non-uniqueness of cohesive-crack stress-separation law of human and bovine bones and remedy by size effect tests, International Journal of Fracture 181 (2013) 67–81. doi:10.1007/S10704-013-9821-8.

[29] R. K. Nalla, J. J. Kruzic, R. O. Ritchie, On the origin of the toughness of mineralized tissue: microcracking or crack bridging?, Bone 34 (2004) 790–798. doi:10.1016/J.BONE.2004.02.001.

[30] M. J. Mirzaali, J. J. Schwiedrzik, S. Thaiwichai, J. P. Best, J. Michler, P. K. Zysset, U. Wolfram, Mechanical properties of cortical bone and their relationships with age, gender, composition and microindentation properties in the elderly, Bone 93 (2016) 196–211. doi:10.1016/J.BONE.2015.11.018.

[31] H. M. Britz, C. D. L. Thomas, J. G. Clement, D. M. Cooper, The relation of femoral osteon geometry to age, sex, height and weight, Bone 45 (2009) 77–83. doi:10.1016/J.BONE.2009.03.654.

[32] M. A. Gallant, D. M. Brown, M. Hammond, J. M. Wallace, J. Du, A. C. Deymier-Black, J. D. Almer, S. R. Stock, M. R. Allen, D. B. Burr, Bone cell-independent benefits of raloxifene on the skeleton: A novel mechanism for improving bone material properties, Bone 61 (2014) 191–200. doi:10.1016/J.BONE.2014.01.009.

[33] F. N. Schmidt, M. Hahn, K. E. Stockhausen, T. Rolvien, C. Schmidt, T. Knopp, C. Schulze, K. Püschel, M. Amling, B. Busse, Influence of x-rays and gamma-rays on the mechanical performance of human bone factoring out intraindividual bone structure and composition indices, Materials Today Bio 13 (2022) 100169. doi:10.1016/J.MTBIO.2021.100169.

[34] G. V. Guinea, J. Planas, M. Elices, Stress intensity factor, compliance and cmod for a general three-point-bend beam, International Journal of Fracture 89 (1998) 103–116. doi:10.1023/A:1007498132504.

[35] Z. P. Bažant, M. T. Kazemi, Size dependence of concrete fracture energy determined by rilem work-of-fracture method, International Journal of Fracture 51 (1991) 121–138. doi:10.1007/BF00033974.

[36] Z. P. Bazant, M. T. Kazemi, Determination of fracture energy, process zone longth and brittleness number from size effect, with application to rock and conerete, International Journal of Fracture 44 (1990) 111–131. doi:10.1007/BF00047063.

[37] B. Busse, H. A. Bale, E. A. Zimmermann, B. Panganiban, H. D. Barth, A. Carriero, E. Vettorazzi, J. Zustin, M. Hahn, J. W. Ager, K. Püschel, M. Amling, R. O. Ritchie, Vitamin d deficiency induces early signs of aging in human bone, increasing the risk of fracture, Science Translational Medicine 5 (2013) 193ra88. doi:10.1126/scitranslmed.3006286.

[38] E. A. Zimmermann, R. O. Ritchie, Bone as a structural material, Advanced Healthcare Materials 4 (2015) 1287–1304. doi:10.1002/ADHM.201500070.

[39] C. M. Bartlow, K. A. Mann, T. A. Damron, M. E. Oest, Limited field radiation therapy results in decreased bone fracture toughness in a murine model, PLOS ONE 13 (2018) e0204928. doi:10.1371/JOURNAL.PONE.0204928.

[40] A. Carriero, E. A. Zimmermann, S. J. Shefelbine, R. O. Ritchie, A methodology for the investigation of toughness and crack propagation in mouse bone, Journal of the Mechanical Behavior of Biomedical Materials 39 (2014) 38–47. doi:10.1016/J.JMBBM.2014.06.017.

[41] D. D. Thompson, Age changes in bone mineralization, cortical thickness, and haversian canal area, Calcified Tissue International 31 (1980) 5–11. doi:10.1007/BF02407161.

[42] S. Khosla, B. L. Riggs, E. J. Atkinson, A. L. Oberg, L. J. McDaniel, M. Holets, J. M. Peterson, L. J. Melton, Effects of sex and age on bone microstructure at the ultradistal radius: A population-based noninvasive

in vivo assessment, Journal of Bone and Mineral Research 21 (2006) 124–131. doi:10.1359/JBMR.050916.

[43] T. Diab, K. W. Condon, D. B. Burr, D. Vashishth, Age-related change in the damage morphology of human cortical bone and its role in bone fragility, Bone 38 (2006) 427–431. doi:10.1016/J.BONE.2005.09.002.

[44] M. Grynpas, Age and disease-related changes in the mineral of bone, Calcified Tissue International 53 (1993) S57–S64. doi:10.1007/BF01673403.

[45] M. Saito, K. Marumo, Collagen cross-links as a determinant of bone quality: A possible explanation for bone fragility in aging, osteoporosis, and diabetes mellitus, Osteoporosis International 21 (2010) 195–214. doi:10.1007/S00198-009-1066-Z.

[46] F. Chen, Z. Wang, T. Bhattacharyya, Absence of femoral cortical thickening in long-term bisphosphonate users: Implications for atypical femur fractures, Bone 62 (2014) 64–66. doi:10.1016/J.BONE.2014.01.011.

[47] R. Niimi, T. Kono, A. Nishihara, M. Hasegawa, A. Matsumine, T. Kono, A. Sudo, Cortical thickness of the femur and long-term bisphosphonate use, Journal of Bone and Mineral Research 30 (2015) 225–231. doi:10.1002/JBMR.2345.

[48] A. Vainionpää, R. Korpelainen, H. Sievänen, E. Vihriälä, J. Leppäluoto, T. Jämsä, Effect of impact exercise and its intensity on bone geometry at weight-bearing tibia and femur, Bone 40 (2007) 604–611. doi:10.1016/J.BONE.2006.10.005.

[49] E. Seeman, P. D. Delmas, D. A. Hanley, D. Sellmeyer, A. M. Cheung, E. Shane, A. Kearns, T. Thomas, S. K. Boyd, S. Boutroy, C. Bogado, S. Majumdar, M. Fan, C. Libanati, J. Zanchetta, Microarchitectural deterioration of cortical and trabecular bone: Differing effects of denosumab and alendronate, Journal of Bone and Mineral Research 25 (2010) 1886–1894. doi:10.1002/JBMR.81.

[50] K. E. Poole, G. M. Treece, A. H. Gee, J. P. Brown, M. R. McClung, A. Wang, C. Libanati, Denosumab rapidly increases cortical bone in key locations of the femur: A 3d bone mapping study in women with

osteoporosis, Journal of Bone and Mineral Research 30 (2015) 46–54. doi:10.1002/JBMR.2325.

[51] R. Zebaze, C. Libanati, M. R. McClung, J. R. Zanchetta, D. L. Kendler, A. Høiseth, A. Wang, A. Ghasem-Zadeh, E. Seeman, Denosumab reduces cortical porosity of the proximal femoral shaft in postmenopausal women with osteoporosis, Journal of Bone and Mineral Research 31 (2016) 1827–1834. doi:10.1002/JBMR.2855.

[52] C. Acevedo, H. Bale, B. Gludovatz, A. Wat, S. Y. Tang, M. Wang, B. Busse, E. A. Zimmermann, E. Schaible, M. R. Allen, D. B. Burr, R. O. Ritchie, Alendronate treatment alters bone tissues at multiple structural levels in healthy canine cortical bone, Bone 81 (2015) 352–363. doi:10.1016/J.BONE.2015.08.002.

[53] M. R. Allen, D. B. Burr, Bisphosphonate effects on bone turnover, microdamage, and mechanical properties: What we think we know and what we know that we don't know, Bone 49 (2011) 56–65. doi:10.1016/J.BONE.2010.10.159.

[54] A. Bernhard, P. Milovanovic, E. A. Zimmermann, M. Hahn, D. Djonic, M. Krause, S. Breer, K. Püschel, M. Djuric, M. Amling, B. Busse, Micro-morphological properties of osteons reveal changes in cortical bone stability during aging, osteoporosis, and bisphosphonate treatment in women, Osteoporosis International 24 (2013) 2671–2680. doi:10.1007/s00198-013-2374-x.

[55] A. Gustafsson, M. Wallin, H. Khayyeri, H. Isaksson, Crack propagation in cortical bone is affected by the characteristics of the cement line: a parameter study using an xfem interface damage model, Biomechanics and Modeling in Mechanobiology 18 (2019) 1247–1261. doi:10.1007/S10237-019-01142-4.

[56] A. Idkaidek, I. Jasiuk, Cortical bone fracture analysis using xfem – case study, International Journal for Numerical Methods in Biomedical Engineering 33 (2017) e2809. doi:10.1002/CNM.2809.

[57] Y. N. Yeni, C. U. Brown, Z. Wang, T. L. Norman, The influence of bone morphology on fracture toughness of the human femur and tibia, Bone 21 (1997) 453–459. doi:10.1016/S8756-3282(97)00173-7.

[58] A. Demirtas, E. A. Taylor, B. Gludovatz, R. O. Ritchie, E. Donnelly, A. Ural, An integrated experimental-computational framework to assess the influence of microstructure and material properties on fracture toughness in clinical specimens of human femoral cortical bone, Journal of the Mechanical Behavior of Biomedical Materials 145 (2023) 106034. doi:10.1016/J.JMBBM.2023.106034.

[59] J. S. Nyman, M. Reyes, X. Wang, Effect of ultrastructural changes on the toughness of bone, Micron 36 (2005) 566–582. doi:10.1016/J.MICRON.2005.07.004.

[60] R. K. Surowiec, R. Saldivar, R. K. Rai, C. E. Metzger, A. M. Jacobson, M. R. Allen, J. M. Wallace, Ex vivo exposure to calcitonin or raloxifene improves mechanical properties of diseased bone through non-cell mediated mechanisms, Bone 173 (2023) 116805. doi:10.1016/J.BONE.2023.116805.

[61] R. F. van Oers, R. Ruimerman, B. van Rietbergen, P. A. Hilbers, R. Huiskes, Relating osteon diameter to strain, Bone 43 (2008) 476–482. doi:10.1016/J.BONE.2008.05.015.

[62] M. Shin, M. Zhang, A. vom Scheidt, M. H. Pelletier, W. R. Walsh, P. J. Martens, J. J. Kruzic, B. Busse, B. Gludovatz, Impact of test environment on the fracture resistance of cortical bone, Journal of the Mechanical Behavior of Biomedical Materials 129 (2022) 105155. doi:10.1016/J.JMBBM.2022.105155.